

# DRBEM Solution of MHD Flow with Magnetic Induction and Heat Transfer

B. Pekmen<sup>1,2</sup> and M. Tezer-Sezgin<sup>2,3</sup>

**Abstract:** This study proposes the dual reciprocity boundary element (DRBEM) solution for full magnetohydrodynamics (MHD) equations in a lid-driven square cavity. MHD equations are coupled with the heat transfer equation by means of the Boussinesq approximation. Induced magnetic field is also taken into consideration. The governing equations in terms of stream function, temperature, induced magnetic field components, and vorticity are solved employing DRBEM in space together with the implicit backward Euler formula for the time derivatives. The use of DRBEM with linear boundary elements which is a boundary discretization method enables one to obtain small sized linear systems. This makes the whole procedure computationally efficient and cheap. The results are depicted with respect to varying physical parameters such as Prandtl ( $0.005 \leq Pr \leq 1$ ), Reynolds ( $100 \leq Re \leq 2500$ ), magnetic Reynolds ( $1 \leq Rem \leq 100$ ), Hartmann ( $10 \leq Ha \leq 100$ ) and Rayleigh ( $10 \leq Ra \leq 10^6$ ) numbers for discussing the effect of each parameter on the flow and temperature behaviors of the fluid. It is found that an increase in  $Ha$  slows down the fluid motion and heat transfer becomes conductive. Centered square blockage causes secondary flows on its left and right even for small  $Re$ . Strong temperature gradients occur around the blockage and near the moving lid for increasing values of  $Ra$ .

**Keywords:** MHD, convection, DRBEM, heat transfer

## 1 Introduction

MHD is a branch of science dealing with the interaction between electromagnetic fields and conducting fluids. It has many applications such as design of cooling systems in nuclear reactors, electromagnetic pumps, MHD generators, etc. MHD flows with buoyancy is also arisen in magnetic field control of nuclear engineering

---

<sup>1</sup> Department of Mathematics, Atılım University, 06836, Ankara, Turkey.

<sup>2</sup> Institute of Applied Mathematics, Middle East Technical University, 06800, Ankara, Turkey.

<sup>3</sup> Department of Mathematics, Middle East Technical University, 06800, Ankara, Turkey.

thermo-hydraulics processes, MHD energy systems, and magneto-plasma dynamics.

Analytically, an exact solution for the hydromagnetic natural convection boundary layer flow is presented past an infinite vertical flat plate in the presence of magnetic field including magnetic induction effects by Ghosh, Bég, and Zueco (2010). Numerical modeling is usually carried on incompressible MHD flows to reduce the complexity of physical problem. In order to simulate the 2D incompressible MHD flow, Peaceman and Rachford alternating-direction implicit (ADI) scheme is performed at low magnetic Reynolds number by Navarro, Cabezas-Gómez, Silva, and Montagnoli (2007). In their study, the solution is obtained in terms of stream function-vorticity-electric current density and magnetic potential. Finite element method (FEM) with some new stabilization techniques is used for solving incompressible MHD equations in Aydin, Neslitürk, and Tezer-Sezgin (2010); Codina and Silva (2006); Gerbeau (2000). The flow of liquid metals in strong magnetic field is analyzed by Sterl (1990). Time integration algorithms which are long-term dissipative and unconditionally stable are examined by Armero and Simo (1996), and they applied the Galerkin mixed FEM to the incompressible MHD equations. Bozkaya and Tezer-Sezgin (2011) have taken into account the current density formulation, and used DRBEM to solve the full MHD problem. Kang and Keyes (2008) compares the two different formulations using FEM with an implicit time integration scheme for incompressible MHD problem in terms of stream function, and a hybrid approach using velocity and magnetic fields to satisfy the divergence-free conditions. FEM is also used for solving 3D MHD flows by Salah, Soulaïmani, and Habashi (2001), and with a stabilization technique in Salah, Soulaïmani, Habashi, and Fortin (1999). Pekmen and Tezer-Sezgin (2013) applied the DRBEM to solve the incompressible MHD flow in a lid-driven cavity, and in a channel with a square cylinder. A steady, laminar, incompressible, viscous flow of an electrically conducting liquid-metal fluid chosen as Gallium-Indium-Tin under the effect of a transverse magnetic field is also investigated in a circular pipe by Gedik, Kurt, and Recebli (2013) using a commercial software.

MHD flow with heat transfer is also an important problem from the physical point of view. Lima and Rêgo (2013) used the generalized integral transform technique (GITT) to solve a MHD channel flow with heat transfer in the entrance region. Alchaar, Vasseur, and Bilgen (1995) presented the combination of a second order finite difference method and ADI method for solving MHD free convection in a shallow cavity heated from below. Al-Najem, Khanafer, and El-Refaae (1998) also studied the laminar natural convection under the effect of an applied magnetic field employing ADI method. In a linearly heated lid-driven cavity, Al-Salem, Oztop, Pop, and Varol (2012) investigated the importance of the moving lid direc-

tion on MHD mixed convection using finite volume method (FVM). They found that heat is transferred much more in the  $+x$ -direction than the  $-x$ -direction for both forced and mixed convection cases. Colaço, Dulikravich, and Orlande (2009) carried out the radial basis function (RBF) approximation for solving the stream function (fourth order)-temperature form of the governing equations of MHD thermal buoyancy flow. It is found that RBF method gives good accuracy with small number of computational grids which makes the procedure computationally cheap. Liquid metal free convection under the influence of a magnetic field in a heated cubic enclosure is solved by a finite volume method (FVM) in Ciofalo and Cricchio (2002). Sentürk, Tessarotto, and Aslan (2009) presented a Lax-Wendroff type matrix distribution scheme combining a dual-time stepping technique with multi-stage Runge-Kutta algorithm to solve the steady/unsteady magnetized/neutral convection problems with the effect of heat transfer. Liquid metal flow in a channel is subjected to external and internal electric and magnetic fields. Abbassi and Nasrallah (2007) investigated the MHD flow with heat transfer in a backward-facing step using a modified control volume FEM using standard staggered grid. The SIMPLER algorithm has been used in terms of velocity-pressure unknowns, and ADI scheme is performed for the time evolution. Mramor, Vertnik, and Sarler (2013) formulated the natural convection flow under a magnetic field neglecting induced magnetic field by meshless local radial basis function collocation method. Mejri, Mahmoud, Abbassi, and Omri (2014) also studied the MHD natural convection performing Lattice Boltzmann method in an enclosure filled with a nano-fluid in which spatially varying sinusoidal temperature boundary conditions on side walls are considered.

The fluid flow and heat transfer characteristics with obstacles inside the cavity are also investigated by some researchers. This configuration has important industrial applications as in geo-physical systems, and convection in buildings with natural cooling flow. Studies are mostly concentrated on obstacles as a circular cylinder inside the enclosure. Some of the numerical studies are as follows. Kim, Lee, Ha, and Yoon (2008) analyzed the importance of the location of a hot circular cylinder on natural convection in a cold square enclosure filled with air using immersed boundary method (IBM). The same problem is also investigated using the finite volume method by Hussain and Hussein (2010) with a uniformly heated circular cylinder immersed in a square enclosure. Using a commercial code FLUENT, mixed convection in a lid-driven enclosure with a circular body is examined also taking into account the conduction equation inside the cylinder in Oztop, Zhao, and Yu (2009). Adding joule heating and magnetic field effects to the system, Rahman, Alim, and Sarker (2010) have shown the significant effect of the cylinder obstacle on the fluid flow using Galerkin finite element method. The energy equation in the solid region

is coupled to momentum and energy equations for the fluid in the cavity.

Some of the numerical schemes for natural and/or mixed convection flows are carried in enclosures containing obstacles of square shape. Ha, Kim, Yoon, Yoon, Lee, Balachandar, and Chun (2002) used the Chebyshev spectral collocation method to observe the natural convection with a square body located at the center of the computational domain for a range of Rayleigh numbers. They have also taken into consideration varying thermal boundary conditions on the square body as cold, neutral, hot isothermal, and adiabatic body conditions. Bhave, Narasimhan, and Rees (2006) analyzed the optimal square body size and the corresponding maximum heat transfer as a function of Rayleigh and Prandtl numbers. Finite volume method has been used for solving mass, momentum and energy equations inside the enclosure when the square blockage was adiabatic. Laminar mixed convection is studied in a square cavity with a heated square blockage immersed using finite volume method in Islam, Sharif, and Carlson (2012). A CFD code ANSYS FLUENT is used for calculations.

In this study, full MHD equations are investigated first in a unit square cavity, and in a cavity with a heated square blockage located at the center. The fluid inside the cavity is viscous, incompressible and electrically, thermally conducting. An external magnetic field with intensity  $B_0$  is applied in  $+y$ -direction. The induced magnetic field equations which are coupled to stream function, vorticity and energy equations are also solved in the fluid region. Numerical results are obtained by using DRBEM which is a boundary-only discretization numerical method. Unconditionally stable backward implicit Euler scheme is used for time integration. It is found that the increase in  $Ha$  slows down the fluid velocity and suppresses the heat transfer inside the cavity. Magnetic Reynolds number does not affect the heat transfer much. Furthermore, the presence of a heated square blockage inside a cold wall square enclosure has a strong effect on isotherms, and induced magnetic field lines are perturbed as  $Ra$  increases. The square solid blockage at the center causes to develop secondary flows through left and right walls of the cavity even for moderate  $Re$ .

## 2 Mathematical Basis

The two-dimensional, unsteady, laminar, incompressible MHD flow and the heat transfer in lid-driven cavities are considered. Joule heating, viscous dissipation, displacement current, convection current and Hall effects are neglected. The problem configurations may be given as in Figures 1(a) and 1(b). The cold wall enclosure containing a heated square blockage located at the center is also examined.

Jagged walls show the adiabatic walls ( $\partial T / \partial n = 0$ ). No-slip condition is imposed

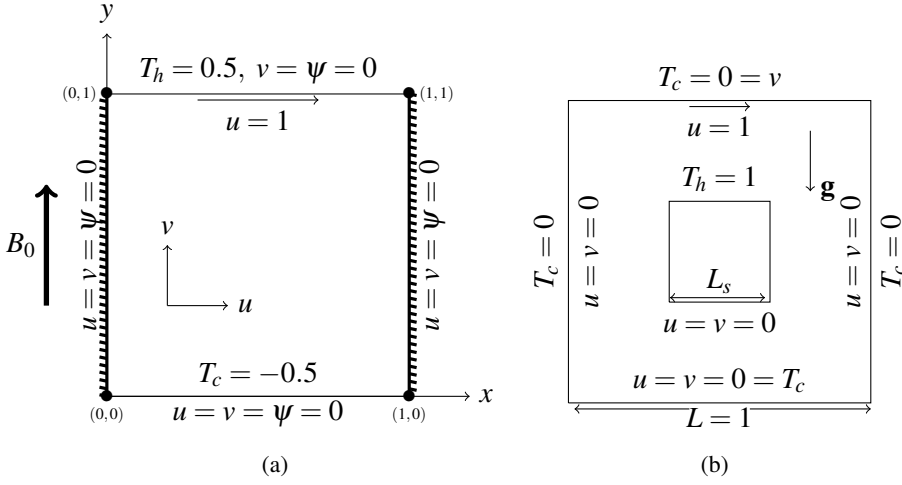


Figure 1: Problem configurations.

on the walls while the top wall moves with a constant velocity  $u = 1$ . Thus, the stream function is set to zero on outer boundaries in both configurations, and it is unknown but a constant on the inner square cylinder (Le-Cao, Mai-Duy, Tran, and Tran-Cong (2011)). This constant value of boundary streamline on the square cylinder is determined considering the streamline values when the square blockage is absent. The vorticity boundary conditions are not known. They are going to be obtained during the solution procedure by using the definition of vorticity and DRBEM coordinate matrix.  $T_h$  and  $T_c$  represent hot and cold walls, respectively, and  $T_s$  is the temperature on the square solid blockage. The externally applied magnetic field with an intensity  $B_0$  is in  $+y$ -direction in both configurations. Induced magnetic field in the fluid is taken into account due to the electrical conductivity of the fluid, however the blockage is assumed to be non-conducting producing negligible induced magnetic field ( $Rem$  is assumed to be very small in the blockage). On both cavity and solid blockage walls  $x$ -component of magnetic field is taken as zero,  $y$ -component as one since external magnetic field is applied in  $y$ -direction. MHD equations are a combination of Navier-Stokes and Maxwell's equations through Ohm's law. In the presence of temperature, the density of the fluid varies according to Boussinesq approximation which is

$$\rho = \rho_0 (1 - \beta(T - T_c)), \tag{1}$$

where  $\rho$  is the density of the fluid,  $\rho_0$  is the reference density,  $T$  is the temperature,  $T_c$  is the reference temperature, and  $\beta$  is the thermal expansion coefficient with  $\beta = -[\partial\rho/\partial T]/\rho$ .

Pre-Maxwell form of the equations in MHD may be given as (Davidson (2001))

$$\nabla \times \mathbf{B} = \mu_m \mathbf{J}, \quad \text{Ampere's Law,} \quad (2)$$

$$\nabla \times \mathbf{E} = -\frac{\partial \mathbf{B}}{\partial t}, \quad \text{Faraday's Law,} \quad (3)$$

$$\mathbf{J} = \sigma (\mathbf{E} + \mathbf{u} \times \mathbf{B}), \quad \text{Ohm's Law,} \quad (4)$$

where  $\mathbf{B} = (B_x, B_y)$  is the total magnetic field,  $\mu_m$  is the magnetic permeability,  $\mathbf{J}$  is the current density,  $\mathbf{E}$  is the electric field,  $\sigma$  is the electrical conductivity.

Once the curl of both sides of Eq.(2) and Eq.(4) is taken, using the identity

$$\nabla \times (\nabla \times \mathbf{B}) = \nabla(\nabla \cdot \mathbf{B}) - \nabla^2 \mathbf{B}, \quad (5)$$

and  $\nabla \cdot \mathbf{B} = 0$ , which is the solenoidal nature of magnetic field, the magnetic field relation

$$-\frac{1}{\mu_m} \nabla^2 \mathbf{B} = \sigma (\nabla \times \mathbf{E} + \nabla \times (\mathbf{u} \times \mathbf{B})), \quad (6)$$

is obtained. Substituting Faraday's law (3) into this relation, the magnetic induction equations may be written as

$$\frac{1}{\mu_m \sigma} \nabla^2 \mathbf{B} = \frac{\partial \mathbf{B}}{\partial t} - \nabla \times (\mathbf{u} \times \mathbf{B}). \quad (7)$$

Continuity and momentum equations for an incompressible and electrically conducting fluid are

$$\nabla \cdot \mathbf{u} = 0 \quad (8)$$

$$\nu \nabla^2 \mathbf{u} = \frac{\partial \mathbf{u}}{\partial t} + \mathbf{u}(\nabla \cdot \mathbf{u}) + \frac{1}{\rho_0} \nabla P + \beta(T - T_c) \mathbf{g} - \mathbf{J} \times \mathbf{B}, \quad (9)$$

where  $\mathbf{u}$  is the velocity field,  $\nu$  is the kinematic viscosity,  $P$  is the pressure. The last two terms are buoyancy body term and Lorentz force due to the externally applied magnetic field, respectively.

The energy equation which gives the temperature variation of the fluid (heat transfer) is

$$\alpha \nabla^2 T = \frac{\partial T}{\partial t} + \mathbf{u} \cdot \nabla T, \quad (10)$$

where  $\alpha$  is the thermal diffusivity of the fluid.

The explicit form of full MHD heat transfer equations in 2-D then, are

$$\frac{\partial u}{\partial x} + \frac{\partial v}{\partial y} = 0 \tag{11}$$

$$v\nabla^2 u = \frac{\partial u}{\partial t} + u\frac{\partial u}{\partial x} + v\frac{\partial u}{\partial y} + \frac{1}{\rho_0}\frac{\partial P}{\partial x} + \frac{B_y}{\rho_0\mu_m}\left(\frac{\partial B_y}{\partial x} - \frac{\partial B_x}{\partial y}\right) \tag{12}$$

$$v\nabla^2 v = \frac{\partial v}{\partial t} + u\frac{\partial v}{\partial x} + v\frac{\partial v}{\partial y} + \frac{1}{\rho_0}\frac{\partial P}{\partial y} - \frac{B_x}{\rho_0\mu_m}\left(\frac{\partial B_y}{\partial x} - \frac{\partial B_x}{\partial y}\right) - g\beta(T - T_c) \tag{13}$$

$$\frac{1}{\sigma\mu_m}\nabla^2 B_x = \frac{\partial B_x}{\partial t} + u\frac{\partial B_x}{\partial x} + v\frac{\partial B_x}{\partial y} - B_x\frac{\partial u}{\partial x} - B_y\frac{\partial u}{\partial y} \tag{14}$$

$$\frac{1}{\sigma\mu_m}\nabla^2 B_y = \frac{\partial B_y}{\partial t} + u\frac{\partial B_y}{\partial x} + v\frac{\partial B_y}{\partial y} - B_x\frac{\partial v}{\partial x} - B_y\frac{\partial v}{\partial y} \tag{15}$$

$$\alpha\nabla^2 T = \frac{\partial T}{\partial t} + u\frac{\partial T}{\partial x} + v\frac{\partial T}{\partial y}. \tag{16}$$

Differentiating Eq.(13) with respect to  $x$ , and Eq.(12) with respect to  $y$ , and subtracting from each other, pressure term is eliminated and vorticity equation is obtained using the continuity condition  $\nabla \cdot \mathbf{u} = 0$ . Further, stream function  $\psi$  is used to satisfy continuity equation defining  $u = \partial\psi/\partial y$ , and  $v = -\partial\psi/\partial x$ .  $\mathbf{B} = (0, B_0)$  is applied on the cavity and blockage walls.

For non-dimensionalization, the following dimensionless variables are defined

$$x' = \frac{x}{L}, \quad y' = \frac{y}{L}, \quad u' = \frac{u}{U_0}, \quad v' = \frac{v}{U_0}, \quad t' = \frac{tU_0}{L}, \quad T' = \frac{T - T_c}{\Delta T}$$

$$p' = \frac{P}{\rho U_0^2}, \quad w' = \frac{wL}{U_0}, \quad \psi' = \frac{\psi}{U_0 L}, \quad B'_x = \frac{B_x}{B_0}, \quad B'_y = \frac{B_y}{B_0},$$

where  $L$  is the characteristic length,  $U_0$  is the characteristic velocity,  $B_0$  is the magnitude of the externally applied magnetic field,  $\Delta T$  is the temperature difference between hot and cold walls.

Dropping the prime notation, the governing non-dimensional equations in terms of stream function  $\psi$ , temperature  $T$ , induced magnetic field components  $B_x$ ,  $B_y$ , and vorticity  $w$  are

$$\nabla^2 \psi = -w \tag{17a}$$

$$\frac{1}{PrRe}\nabla^2 T = \frac{\partial T}{\partial t} + u\frac{\partial T}{\partial x} + v\frac{\partial T}{\partial y} \tag{17b}$$

$$\frac{1}{Rem}\nabla^2 B_x = \frac{\partial B_x}{\partial t} + u\frac{\partial B_x}{\partial x} + v\frac{\partial B_x}{\partial y} - B_x\frac{\partial u}{\partial x} - B_y\frac{\partial u}{\partial y} \tag{17c}$$

$$\frac{1}{Rem} \nabla^2 B_y = \frac{\partial B_y}{\partial t} + u \frac{\partial B_y}{\partial x} + v \frac{\partial B_y}{\partial y} - B_x \frac{\partial v}{\partial x} - B_y \frac{\partial v}{\partial y} \tag{17d}$$

$$\begin{aligned} \frac{1}{Re} \nabla^2 w = & \frac{\partial w}{\partial t} + u \frac{\partial w}{\partial x} + v \frac{\partial w}{\partial y} - \frac{Ra}{PrRe^2} \frac{\partial T}{\partial x} \\ & - \frac{Ha^2}{ReRem} \left[ B_x \frac{\partial}{\partial x} \left( \frac{\partial B_y}{\partial x} - \frac{\partial B_x}{\partial y} \right) + B_y \frac{\partial}{\partial y} \left( \frac{\partial B_y}{\partial x} - \frac{\partial B_x}{\partial y} \right) \right], \end{aligned} \tag{17e}$$

where the Reynolds number  $Re$ , Prandtl number  $Pr$ , magnetic Reynolds number  $Rem$ , Rayleigh number  $Ra$ , and Hartmann number  $Ha$  are defined as

$$Re = \frac{U_0 L}{\nu}, \quad Pr = \frac{\nu}{\alpha}, \quad Rem = \mu_m \sigma U_0 L, \quad Ra = \frac{g \beta \Delta T L^3}{\alpha \nu}, \quad Ha^2 = \frac{B_0^2 L^2 \sigma}{\mu},$$

where  $\mu$  is the dynamic viscosity.  $(B_x, B_y) = (0, 1)$  is the corresponding non-dimensional induced magnetic field boundary conditions on all of the walls.

### 3 Application of DRBEM to the Problem

The dual reciprocity boundary element method treats the equations (17) as Poisson equations assuming the right hand sides as inhomogeneity in each equation. Then, these inhomogeneous terms are approximated by using radial basis functions, usually polynomials  $f = 1 + r + \dots + r^n$  which are related to Laplacian with particular solutions  $\hat{u}$  as  $\nabla^2 \hat{u} = f$ . Thus, fundamental solution of Laplace equation is used obtaining boundary integral equations corresponding to each differential equation in (17).

Concerning only the diffusion terms on the left hand side of Eqs.(17), the right hand side terms are approximated by a series of radial basis functions  $f_j$  as (Partridge, Brebbia, and Wrobel (1992))

$$\nabla^2 \varphi = b = \sum_{j=1}^{N+L} \alpha_j f_j, \tag{18}$$

where  $\varphi$  denotes either  $\psi, T, B_x, B_y$  or  $w$ ,  $\alpha_j$ 's are sets of initially unknown coefficients,  $N$  is the number of boundary nodes, and  $L$  is the number of arbitrarily taken interior points. The radial basis functions  $f_j$ 's are usually chosen as polynomials of radial distance  $r_{ij}$  as  $f_{ij} = 1 + r_{ij} + r_{ij}^2 + \dots + r_{ij}^n$  where  $i$  and  $j$  correspond to the source(fixed) and the field(variable) points, respectively.

Multiplying both sides of this relation (18) by the fundamental solution  $u^* = \frac{1}{2\pi} \ln \left( \frac{1}{r} \right)$  of Laplace equation, and then integrating over the domain, a domain integral equation is obtained. With the help of Green's identities, all the domain integrals are

transformed to the boundary integrals as

$$c_i \varphi_i + \int_{\Gamma} \varphi \frac{\partial u^*}{\partial n} d\Gamma - \int_{\Gamma} \frac{\partial \varphi}{\partial n} u^* d\Gamma = \sum_{j=1}^{N+L} \alpha_j \left( c_i \hat{u}_{ij} + \int_{\Gamma} \hat{u}_j \frac{\partial u^*}{\partial n} d\Gamma - \int_{\Gamma} \hat{q}_j u^* d\Gamma \right) \quad (19)$$

where  $\varphi$  again denotes either  $\psi, T, B_x, B_y$  or  $w$ ,  $c_i = 1/2$  on the boundary  $\Gamma$  when it is a straight line, and  $c_i = 1$  when the node  $i$  is inside.  $\partial/\partial n$  indicates the normal derivative.

These boundary integrals are discretized using linear boundary elements which result in matrix-vector equations corresponding to each Eqs.(17) as

$$H\varphi - G\varphi_q = (H\hat{U} - G\hat{Q})\alpha, \quad (20)$$

where  $H$  and  $G$  are BEM matrices containing the boundary integrals of  $u^*$  and  $q^* = \partial u^*/\partial n$  evaluated at the nodes, respectively. The vectors  $\varphi$  and  $\varphi_q = \partial\varphi/\partial n$  represent the known and unknown information at the nodes of  $\psi, T, B_x, B_y$  or  $w$ .  $\hat{U}$  and  $\hat{Q}$  are constructed from  $\hat{u}_j$  and then  $\hat{q}_j = \partial\hat{u}_j/\partial n$  columnwise, and are matrices of size  $(N+L) \times (N+L)$ . The vector  $\alpha$  may be deduced from the Eq.(18) as  $\alpha = F^{-1}b$ . Here,  $F$  is the coordinate matrix of size  $(N+L) \times (N+L)$ , and contains radial basis functions  $f_j$ 's as columns evaluated at  $N+L$  points.  $b$  is the vector containing collocated values of the inhomogeneity  $b$  in each equation of (17).

The space derivatives in vector  $b$  are employed by using the coordinate matrix  $F$  while the time derivatives are discretized with Backward-Euler finite difference formula. Thus, the iteration with respect to time for  $\psi, T, B_x, B_y$ , and  $w$  may be given as

$$H\psi^{m+1} - G\psi_q^{m+1} = -S_w^m \quad (21)$$

$$u^{m+1} = D_y \psi^{m+1}, \quad v^{m+1} = -D_x \psi^{m+1} \quad (22)$$

$$\left( H - \frac{PrRe}{\Delta t} S - PrReSM \right) T^{m+1} - GT_q^{m+1} = -\frac{PrRe}{\Delta t} ST^m \quad (23)$$

$$\begin{aligned} & \left( H - \frac{Rem}{\Delta t} S - RemSM + RemSD_x[u]_d^{m+1} \right) B_x^{m+1} - GB_{xq}^{m+1} \\ & = -\frac{Rem}{\Delta t} SB_x^m - RemS[B_y]_d^m D_y u^{m+1} \end{aligned} \quad (24)$$

$$\begin{aligned} & \left( H - \frac{Rem}{\Delta t} S - RemSM + RemSD_y[v]_d^{m+1} \right) B_y^{m+1} - GB_{yq}^{m+1} \\ & = -\frac{Rem}{\Delta t} SB_y^m - RemS[B_x]_d^m D_x v^{m+1} \end{aligned} \quad (25)$$

$$\begin{aligned} & \left( H - \frac{Re}{\Delta t} S - ReSM \right) w^{m+1} - Gw_q^{m+1} \\ &= -\frac{Re}{\Delta t} Sw^m - \frac{Ha^2 S}{Rem} ([B_x]_d^{m+1} D_x \{\zeta\} + [B_y]_d^{m+1} D_y \{\zeta\}) - \frac{Ra}{PrRe} SD_x T^{m+1} \end{aligned} \tag{26}$$

where

$$S = (H\hat{U} - G\hat{Q})F^{-1}, \quad D_x = \frac{\partial F}{\partial x}F^{-1}, \quad D_y = \frac{\partial F}{\partial y}F^{-1}$$

$$M = [u]_d^{m+1} D_x + [v]_d^{m+1} D_y, \quad \{\zeta\} = D_x B_y^{m+1} - D_y B_x^{m+1},$$

$[B_x]_d^{m+1}, [B_y]_d^{m+1}, [u]_d^{m+1}, [v]_d^{m+1}$  enter into the system as diagonal matrices of size  $(N + L) \times (N + L)$ , and  $m$  shows the iteration step. The resulting systems of equations in the form  $Ax = b$ , which are obtained by shuffling the known and unknown information of  $\psi, T, B_x, B_y$ , and  $w$  on the boundary, are solved by Gaussian elimination with partial pivoting.

Initially,  $w^0, B_x^0, B_y^0, T^0$  are taken as zero everywhere (except on the boundary). Once the stream function is computed from Eq.(21), velocity components are determined by Eq.(22) inserting the boundary conditions. Then, temperature equation (23) and induction equations (24)-(25) are solved with the insertion of their boundary conditions. Vorticity boundary conditions are computed by using the definition  $w = \partial v / \partial x - \partial u / \partial y$  with the help of coordinate matrix  $F$  as

$$w_b = \frac{\partial F}{\partial x} F^{-1} v - \frac{\partial F}{\partial y} F^{-1} u. \tag{27}$$

Then, the vorticity transport equation (26) is solved by using these vorticity boundary conditions. The solution process continues in this way until the criterion

$$\sum_{k=1}^5 \frac{\|\varphi_k^{m+1} - \varphi_k^m\|_\infty}{\|\varphi_k^{m+1}\|_\infty} < \varepsilon = 1e-4 \tag{28}$$

is satisfied where  $\varphi_k$  stands for  $\psi, T, B_x, B_y$  and  $w$  values at the boundary and interior points, respectively, and  $m$  indicates the iteration step.

#### 4 Numerical Results

The radial basis function  $f = 1 + r$  is used in the construction of coordinate matrix  $F$  and  $\hat{U}, \hat{Q}$  matrices. 16–point Gaussian quadrature is made use of for the integrals in the BEM matrices  $H$  and  $G$ . In general,  $N = 120$  boundary elements,  $L = 840$  interior points in the ‘lid-driven square cavity problem’, and  $N = 208, L = 880$  in the problem of the ‘cavity with a centered square blockage’ are used, respectively.

Naturally, one needs to take more elements (or interior points) or smaller time increment  $\Delta t$  for increasing large values of physical parameters. The depicted contours (in Figs.3-7, Figs.9-10, Figs.12-13) from left to right are streamlines, isotherms, vorticity lines, and induced magnetic field vector  $(B_x, B_y)$  at steady-state.

Once the vorticity equation Eq.(26) is solved, in order to accelerate the convergence of vorticity which is rather difficult to converge than the other unknowns, a relaxation parameter  $0 < \gamma < 1$  is used as  $w^{m+1} \leftarrow \gamma w^{m+1} + (1 - \gamma)w^m$  for large values of parameters in reaction terms.

The presented numerical procedure is validated in terms of both the graphs of the flow and quantitative results on average Nusselt number on the heated wall. For this, the governing equations are solved neglecting the induced magnetic field as in the case of Colaço, Dulikravich, and Orlande (2009). Figure 2 shows the good agreement in terms of streamlines and isotherms with the results given in Colaço, Dulikravich, and Orlande (2009). Also, the average Nusselt numbers  $(\overline{Nu} = -\int_0^1 (\partial T / \partial x) dy)$  are in good agreement with the ones computed in Colaço, Dulikravich, and Orlande (2009). The computational cost (CPU time in seconds) of the present study is naturally less than the domain discretization methods due to the use of boundary elements only as can be seen in Table 1 (e.g.  $15 \times 15$  grid, 56 boundary elements only).

Table 1: CPU times and  $\overline{Nu}$  on the heated wall with  $Re = 1$ ,  $Pr = 0.71$ ,  $Gr = 10^4$ ,  $\Delta t = 0.01$ .

Ha	Present Study				Colaço, Dulikravich, and Orlande (2009)	
	15 × 15		25 × 25		15 × 15	
	$\overline{Nu}$	CPU	$\overline{Nu}$	CPU	$\overline{Nu}$	CPU
0	2.17	2.59	2.08	37.92	2.02	50.60
10	1.82	3.15	1.74	95.43	1.70	34.03
25	1.20	4.52	1.18	61.51	1.17	42.59
50	1.01	4.76	1.01	59.55	0.97	25.53

Firstly, the problem of MHD flow and heat transfer is solved in a square enclosure (Figure 1(a)). Then, the same problem in a square enclosure with a square blockage is considered (Figure 1(b)). Since the laminar flow is taken into account, Reynolds number value is taken up to 2500. And, the ranges for the other non-dimensional parameters are  $1 \leq Re_m \leq 100$ ,  $Ha \leq 100$ ,  $10 \leq Ra \leq 10^6$ ,  $0.005 \leq Pr \leq 1$ .

As  $Re$  increases (Figure 3), the center of the streamlines in the direction of moving lid shifts through the center of the cavity forming new secondary eddies at the

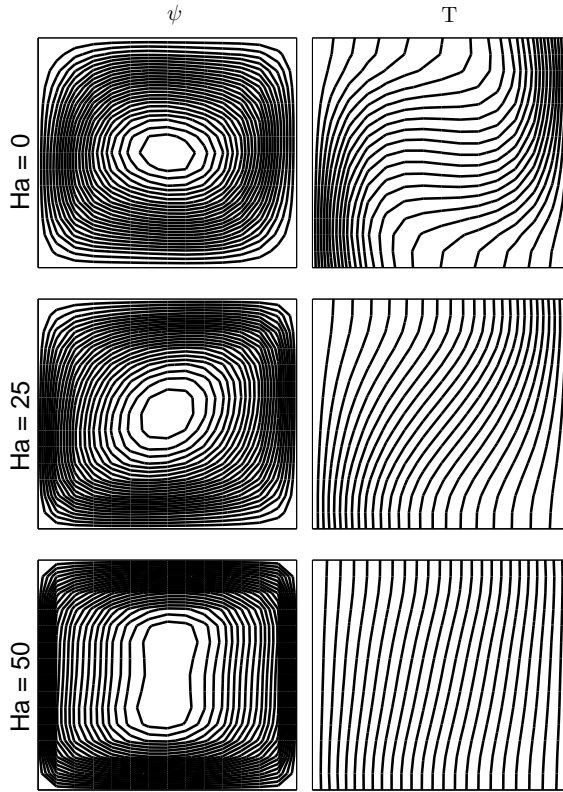


Figure 2: Streamlines and Isotherms with  $Ha$  variation,  $Pr = 0.71$ ,  $Re = 1$ ,  $Gr = 10^4$ .

bottom corners. The dominance of convection is observed in isotherms forming the strong temperature gradients clustered at the top left and bottom right corners. Vorticity is transported inside the cavity forming boundary layers on the top moving lid and right wall close to the upper corner. This shows the concentration of flow through upper right corner. Induced magnetic field is not affected much with the increase in  $Re$ .

With an increase in  $Ha$  (Figure 4), fluid flows slowly due to the retarding effect of Lorentz force. Two new cells on the right and left parts of cavity are observed in streamlines. Heat is transferred by conduction as can be seen from isotherms. Induced magnetic field lines become perpendicular to horizontal walls due to the decrease in the dominance of convection terms in the induction equations. Also, this points to the dominance of external magnetic field which is in the  $+y$ -direction. Vorticity concentrates completely near on the wall with the moving lid being stag-

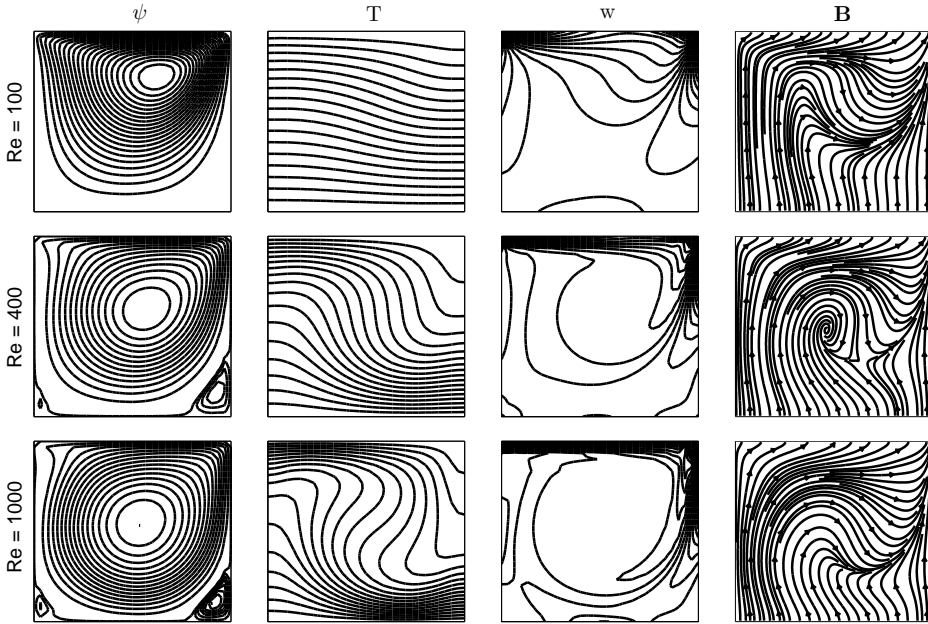


Figure 3:  $Rem = 100$ ,  $Ra = Ha = 10$ ,  $Pr = 0.1$ ,  $\Delta t = 0.25$ .

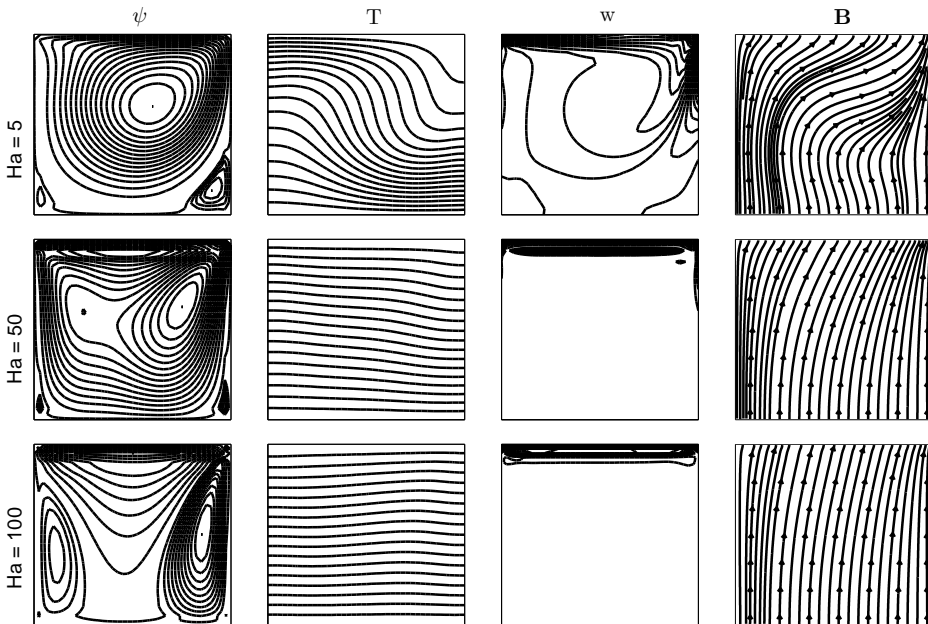


Figure 4:  $Rem = 40$ ,  $Re = 400$ ,  $Ra = 1000$ ,  $Pr = 0.1$ ,  $\Delta t = 0.5$  ( $Ha = 5$ ),  $\Delta t = 0.2$  ( $Ha = 50$ ),  $\Delta t = 0.1$  with  $\gamma = 0.1$  ( $Ha = 100$ ).

nant at the center as the intensity of magnetic field increases (i.e.  $Ha$  increases).

An increase in magnetic Reynolds number  $Rem$  has a great influence on the induced magnetic field only. It shows circulation at the center of the cavity due to the dominance of convection terms in the induction equations, and the effect of external magnetic field diminishes (Figure 5).

As  $Ra$  increases (Figure 6), the isotherms indicate the conduction dominated effect due to the dominance of the buoyancy force. Small counter-clockwise eddy in streamlines with  $Ra = 10^3$  occupies the mid-part of the cavity with  $Ra = 10^4$ , and one more clockwise cell emerges through the bottom part of the cavity as  $Ra$  reaches to the value  $Ra = 10^5$ .

Isotherms circulate inside the cavity pointing to the convective heat transfer with the increase in dominance of convective terms in energy equation as  $Pr$  increases (Figure 7). Not much of a variation in streamlines, vorticity, and induced magnetic field lines is observed.

Secondly, MHD mixed convection flow is solved in a cavity with a square blockage at the center. The centered square cylinder is of size  $L_s = 0.25$ . Inside the solid blockage induced magnetic field is neglected due to the small values of  $Rem$  (small magnetic permeability of the solid). Heat transfer inside the blockage is also neglected due to the small value of thermal diffusivity of the solid and its isothermal structure.  $\psi = -0.05$  is taken on the blockage walls by looking at the average  $\psi$  value at the center of the cavity in the absence of blockage and heat transfer.

Figure 8 shows that our results using DRBEM in solving the mixed convection in a lid-driven cavity with a square blockage, are consistent with the results in Islam, Sharif, and Carlson (2012) (in terms of Richardson number  $Ri = Ra/(PrRe^2)$ ). Blockage causes the secondary flow to develop at a lower value of  $Re$  compared to cavity without blockage. With the increase in  $Re$ , the center of the streamlines which is close to the moving lid again moves to the center of the cavity but to the right of the blockage (Figure 9). Meantime, secondary flow becomes prominent close to the left wall of the cavity. Isotherms are not altered much. But, for large values of  $Re$ , a boundary layer is pronounced on the left and bottom walls of the square blockage due to the secondary flow on the left wall of the cavity. Vorticity is transported inside the cavity as  $Re$  increases. Induced magnetic field vector tending to the direction of moving lid is not affected much.

As  $Ha$  increases (Figure 10), due to the  $+y$ -directed applied magnetic field, the center of the primary cell in streamlines shift through the center of the cavity nearly conflicting with the square blockage. Further, the secondary flow at the left wall of the cavity becomes smaller, and a tertiary flow emerges at the top wall. Not much effect of  $Ha$  on isotherms is observed. This may be due to the small number of  $Pr$ .

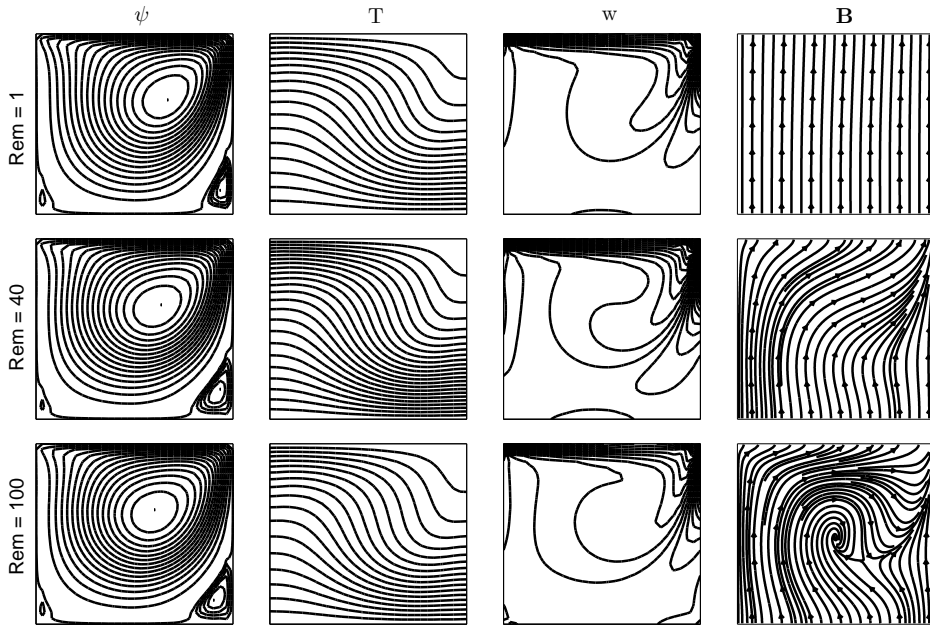


Figure 5:  $Re = 400$ ,  $Ha = 10$ ,  $Ra = 1000$ ,  $Pr = 0.1$ ,  $\Delta t = 0.25$ .

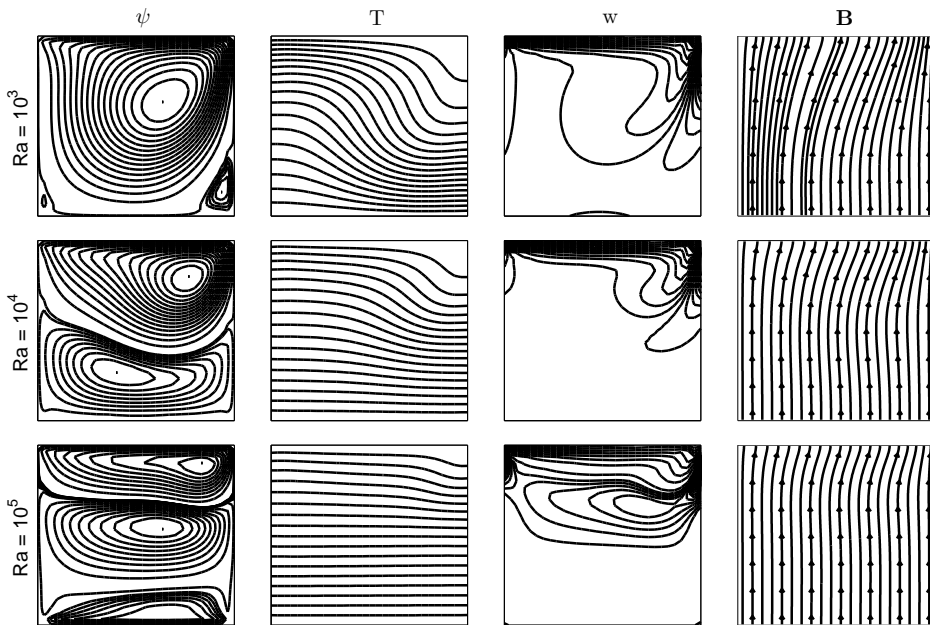


Figure 6:  $Re = 400$ ,  $Rem = Ha = 10$ ,  $Pr = 0.1$ ,  $\Delta t = 0.25$ .

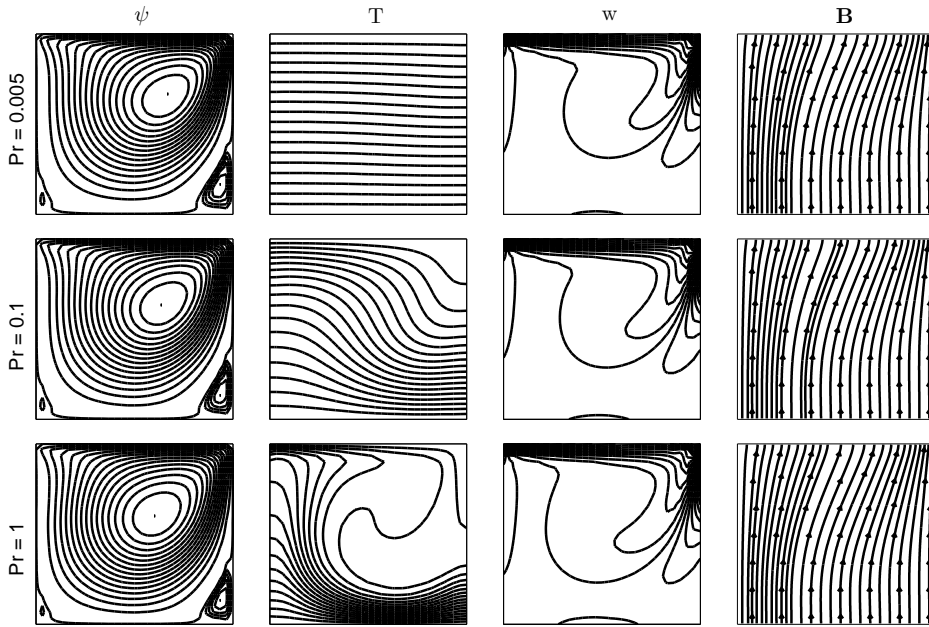


Figure 7:  $Re = 400$ ,  $Rem = Ha = 10$ ,  $Ra = 10^3$ ,  $\Delta t = 0.5$  ( $Pr = 0.005$ ,  $Pr = 0.1$ ),  $\Delta t = 0.25$  ( $Pr = 1$ ).

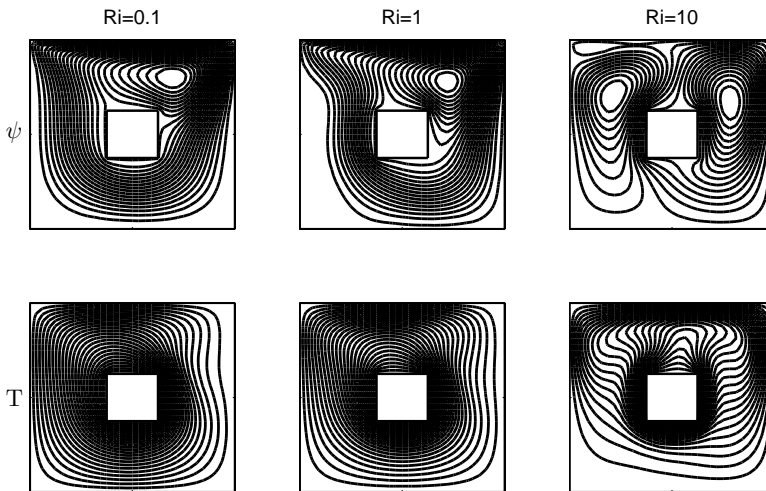


Figure 8: Streamlines and isotherms in terms of Richardson variation,  $Pr = 0.71$ ,  $Re = 100$ ,  $L_s = 0.25$ .

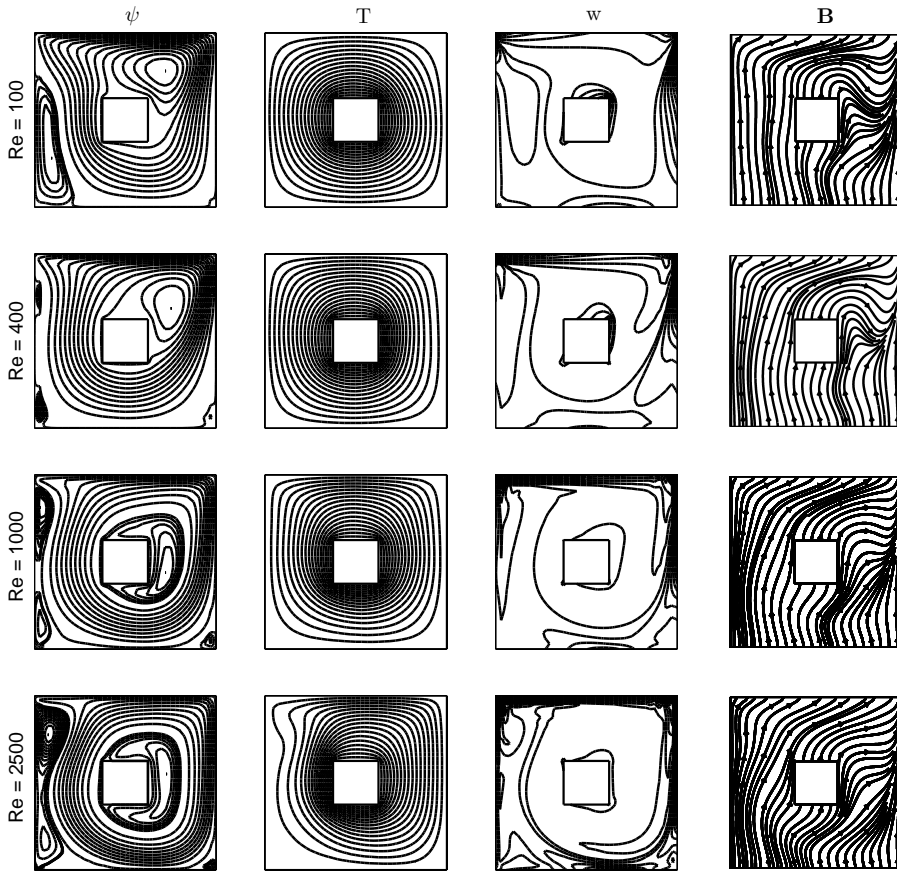


Figure 9:  $Rem = 100$ ,  $Ha = 10$ ,  $Pr = 0.1$ ,  $Ra = 10^3$ ,  $\Delta t = 0.25$  ( $Re = 100, 400, 1000$ ),  $\Delta t = 0.1$  ( $Re = 2500$ ).

Strongly applied magnetic field (large  $Ha$ ) directs the induced magnetic field lines in its direction. This is why  $Rem = 100$  has been taken to start with a turbulence at the right upper corner with small  $Ha$ .

The aim of the second example (MHD convection in a square cavity with a blockage at the center) is to examine the effects of both external magnetic field and the blockage in the cavity. Thus, the streamline value on the blockage walls is exposed to the change as  $Ha$  increases. This is depicted in Figure 11. As can be seen in Figure 11(a), clockwise directed primary cell is divided into two parts and squeezed through the left and right walls, and a counter-rotating cell is intensified covering the center of the cavity as  $Ha$  increases. Thus, the value of stream function changes,

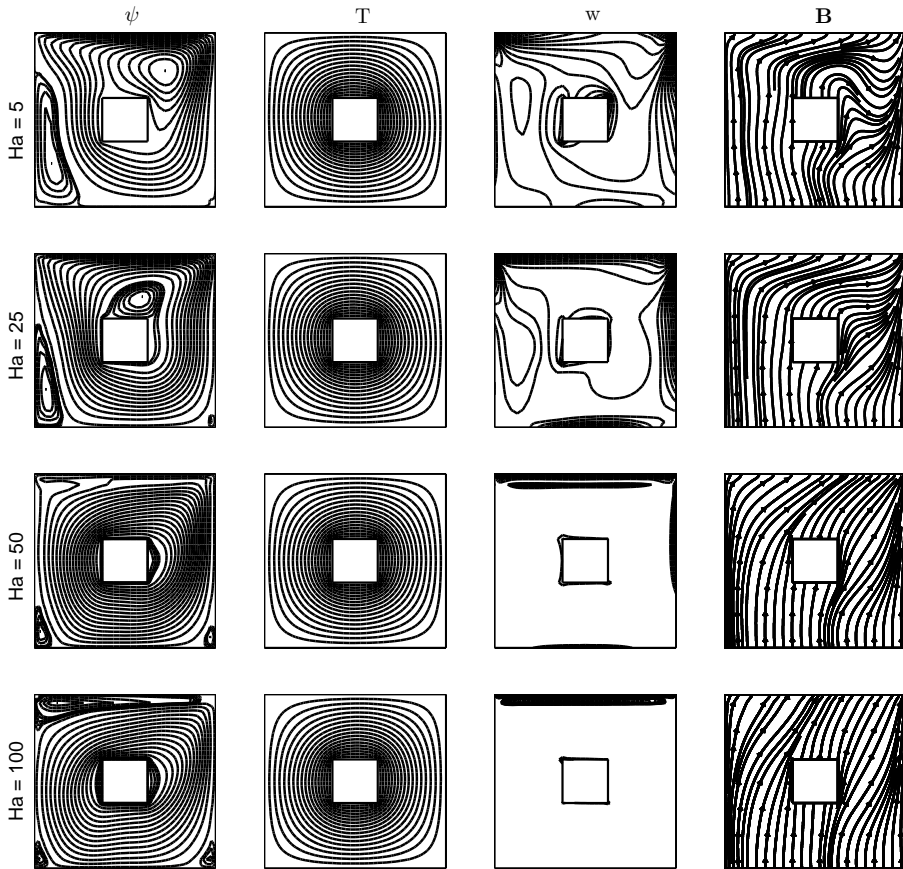
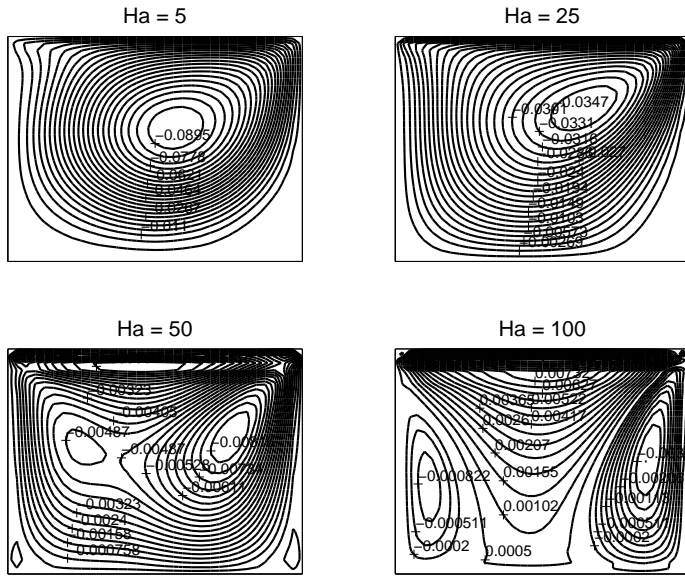
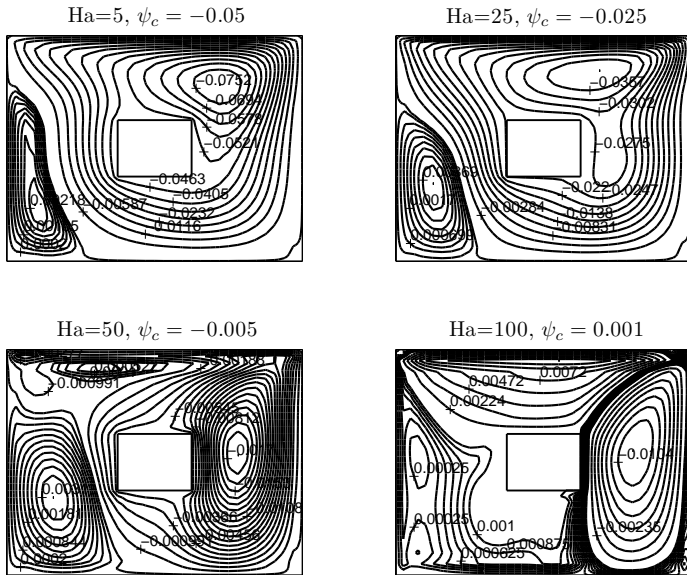


Figure 10:  $Re = Rem = 100$ ,  $Ra = 10^3$ ,  $Pr = 0.1$ ,  $\Delta t = 0.25$  ( $Ha = 5$ ,  $Ha = 25$ ),  $\Delta t = 0.25$  with  $\gamma = 0.5$  ( $Ha = 50$ ),  $\Delta t = 0.1$  with  $\gamma = 0.1$  ( $Ha = 100$ ).

especially at the center of the cavity. Due to this change in the flow, the stream function value which is denoted by  $\psi_c$  on the square obstacle is taken accordingly with the values shown in Figure 11(a). Then, the effects of both applied magnetic field and blockage placed in the center of the cavity, on the flow are shown in Figure 11(b). It is observed that secondary flow developed with  $Ha = 5$  through the left wall becomes larger, and the center of the primary cell shifts through the right wall. Further, the primary cell is pronounced between the right wall of the obstacle and the right wall of the cavity while a counter-rotating cell emerges from top wall of the cavity to the top wall of the square blockage. Retarding effect of Lorentz force starts much earlier (even with  $Ha = 5$ ) and gives symmetric secondary flow cells on the left and right of the blockage when  $Ha = 50$ . Further, the increase in  $Ha$



(a) Without Square Blockage



(b) With Square Blockage

Figure 11: Observation on Streamlines,  $Re = Rem = 100$ ,  $Ra = 10^3$ ,  $Pr = 0.1$ .

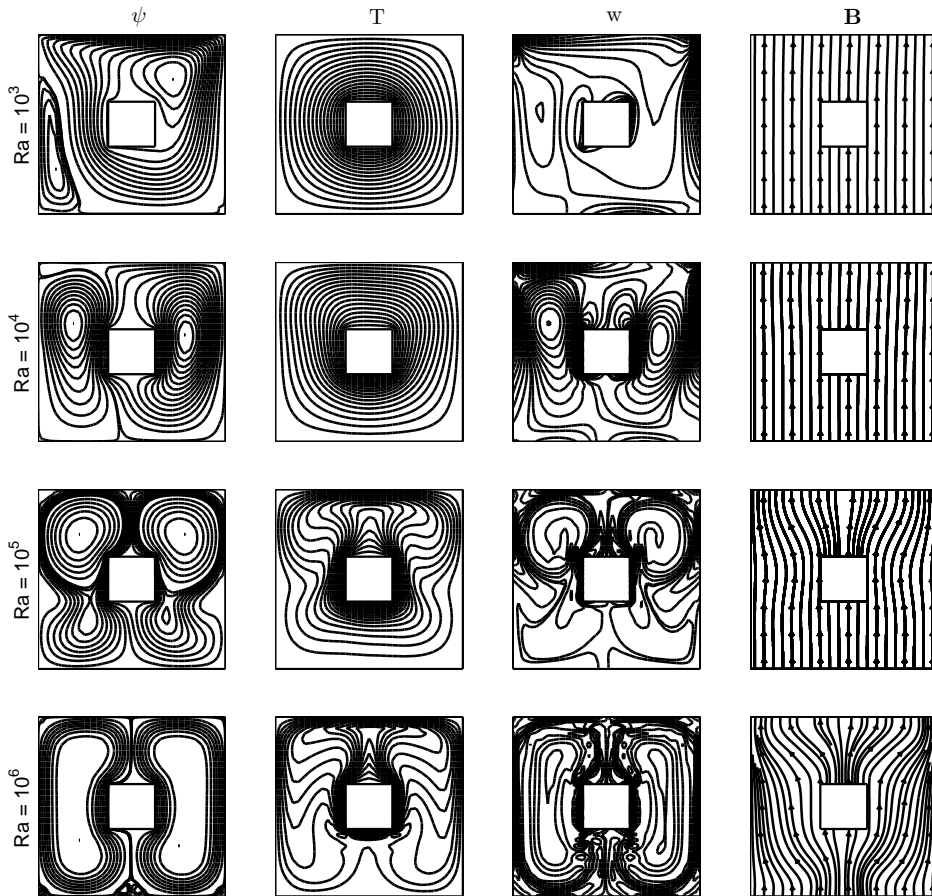


Figure 12:  $Re = 100$ ,  $Rem = 1$ ,  $Ha = 10$ ,  $Pr = 0.1$ ,  $\Delta t = 0.25$  ( $Ra = 10^3$ ,  $Ra = 10^4$ ),  $\Delta t = 0.1$  ( $Ra = 10^5$ ),  $\Delta t = 0.01$  with  $\gamma = 0.1$  ( $Ra = 10^6$ ).

( $Ha = 100$ ) squeezes all the flow cells to the boundaries of the cavity. This is the well known boundary layer formation in the flow for large  $Ha$ .

For  $Ra = 10^3$ , the center of the primary cell is seen through the moving lid and a secondary flow is observed at the left bottom corner of the cavity. With  $Ra = 10^4$ , the primary cell is shrunk through the right mid part while the secondary flow occupies the left part of the cavity. A symmetric behavior in streamlines starts to be pronounced vanishing the effect of moving lid with  $Ra = 10^5$  and  $10^6$ . Vorticity

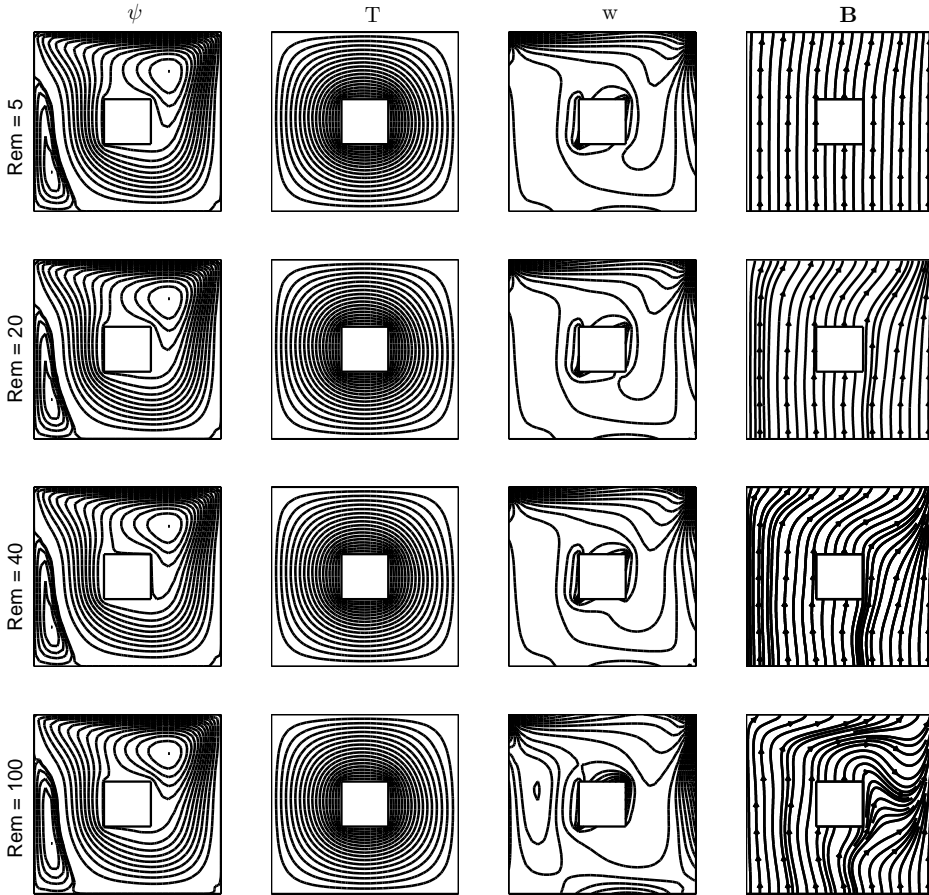


Figure 13:  $Re = 100$ ,  $Ha = 10$ ,  $Pr = 0.1$ ,  $Ra = 10^3$ ,  $\Delta t = 0.25$ .

shows a similar behavior to streamlines as  $Ra$  increases. This is the common effect of large  $Ra$  values on the flow. Furthermore, isotherms also start to be circulated from hot blockage to the cold walls forming strong temperature gradient through the top wall due to the increase in natural convection (buoyancy). Induced magnetic field lines are also affected with the increase in  $Ra$ , and perturbation in opposite directions from square blockage to the top wall is observed. Here,  $Rem = 1$  is purposely taken to observe the effect of the solid blockage for large  $Ra$  (Figure 12). As expected, the variation of  $Rem$  has the influence only on the induced magnetic field lines as can also be seen in Figure 13. Induced magnetic field lines obey the direction of moving lid with the increase in  $Rem$  while the square blockage squeezes them between the blockage and the right wall of the cavity.

## 5 Conclusion

In this article, MHD flow with heat transfer is studied numerically in a square cavity, and a cavity with a centered square blockage. Without square blockage, isotherms form strong temperature gradient through the top and bottom walls pointing to the dominance of convective heat transfer as  $Re$  increases. As expected, the counter-rotating cells emerge and the dominance of conduction is pronounced with the increase in  $Ra$ . The convective heat transfer is revealed as  $Pr$  increases. When  $Ha$  is increased, the conductive heat transfer is seen on isotherms. With centered square blockage, secondary flow becomes prominent close to the left wall of the cavity and right to the blockage. Rising of heat from hot blockage to the cold walls of cavity increases formation of the strong temperature gradients around the blockage and near the moving lid for large values of  $Ra$ . Even with small values of  $Ha$ , secondary flows start and locate through the right and left of the blockage. In both cases, increasing  $Ha$  slows down the fluid motion due to the restraining effect of Lorentz force, and make the induced magnetic field lines perpendicular to the vertical walls since the external magnetic field is applied in  $+y$ -direction. Furthermore, the increase in magnetic Reynolds number  $Rem$  causes the induced magnetic field lines to circulate inside the cavity. Not much effect of  $Rem$  on the heat transfer is observed.

The utilized numerical method DRBEM has the advantage of using small number of boundary nodes which result in small systems. Furthermore, all the space derivatives are easily computed with the BEM coordinate matrix. Thus, the computational cost is much more reasonable than the other domain discretization methods. However, physical problems which need very fine discretisation according to the domain of interest (e.g.domains containing narrow passages, curved pipes) will result in very large sized full systems.

## References

- Abbassi, H.; Nasrallah, B. S.** (2007): MHD flow and heat transfer in a backward-facing step. *International Communications in Heat and Mass Transfer*, vol. 34, pp. 231–237.
- Al-Najem, N.; Khanafer, K.; El-Refae, M.** (1998): Numerical study of laminar natural convection in tilted enclosure with transverse magnetic field. *International Journal of Numerical Methods for Heat and Fluid Flow*, vol. 8, pp. 651–672.
- Al-Salem, K.; Oztop, H. F.; Pop, I.; Varol, Y.** (2012): Effect of moving lid direction on MHD mixed convection in a linearly heated cavity. *International Journal of Heat and Mass Transfer*, vol. 55, pp. 1103–1112.

**Alchaar, S.; Vasseur, P.; Bilgen, E.** (1995): The effect of a magnetic field on natural convection in a shallow cavity heated from below. *Chemical Engineering Communications*, vol. 134, pp. 195–209.

**Armero, F.; Simo, J. C.** (1996): Long-term dissipativity of time-stepping algorithms for an abstract evolution equation with applications to the incompressible MHD and Navier-Stokes equations. *Computer Methods in Applied Mechanics and Engineering*, vol. 131, pp. 41–90.

**Aydin, S. H.; Neslitürk, A. I.; Tezer-Sezgin, M.** (2010): Two-level finite element method with a stabilizing subgrid for the incompressible MHD equations. *International Journal for Numerical Methods in Fluids*, vol. 62, pp. 188–210.

**Bhave, P.; Narasimhan, A.; Rees, D. A. S.** (2006): Natural convection heat transfer enhancement using adiabatic block: Optimal block size and Prandtl number effect. *International Journal of Heat and Mass Transfer*, vol. 49, pp. 3807–3818.

**Bozkaya, N.; Tezer-Sezgin, M.** (2011): The DRBEM solution of incompressible MHD flow equations. *International Journal for Numerical Methods in Fluids*, vol. 67, pp. 1264–1282.

**Ciofalo, M.; Cricchio, F.** (2002): Influence of a magnetic field on liquid metal free convection in an internally heated cubic enclosure. *International Journal of Heat and Fluid Flow*, vol. 12, pp. 687–715.

**Codina, R.; Silva, H. N.** (2006): Stabilized finite element approximation of the stationary magneto-hydrodynamics equations. *Computational Mechanics*, vol. 38, pp. 344–355.

**Colaço, M. J.; Dulikravich, G. S.; Orlande, H. R. B.** (2009): Magnetohydrodynamic simulations using radial basis functions. *International Journal of Heat and Mass Transfer*, vol. 52, pp. 5932–5939.

**Davidson, P. A.** (2001): *An Introduction to Magnetohydrodynamics*. Cambridge University Press.

**Gedik, E.; Kurt, H.; Recebli, H.** (2013): CFD Simulation of Magnetohydrodynamic Flow of a Liquid-Metal Galinstan Fluid in Circular Pipes. *CMES - Computer Modeling in Engineering and Sciences*, vol. 9, pp. 23–33.

**Gerbeau, J. F.** (2000): A stabilized finite element method for the incompressible magnetohydrodynamic equations. *Numerische Mathematik*, vol. 87, pp. 83–111.

**Ghosh, S. K.; Bégu, O. A.; Zueco, J.** (2010): Hydromagnetic free convection flow with induced magnetic field effects. *Meccanica*, vol. 45, pp. 175–185.

**Ha, M. Y.; Kim, I. K.; Yoon, H. S.; Yoon, K. S.; Lee, J. R.; Balachandar, S.; Chun, H. H.** (2002): Two-dimensional and Unsteady Natural Convection in

A Horizontal Enclosure with a Square Body. *Numerical Heat Transfer, Part A: Applications*, vol. 41, pp. 183–210.

**Hussain, S. H.; Hussein, A. K.** (2010): Numerical investigation of natural convection phenomena in a uniformly heated circular cylinder immersed in square enclosure filled with air at different vertical locations. *International Communications in Heat and Mass Transfer*, vol. 37, pp. 1115–1126.

**Islam, A. W.; Sharif, M. A. R.; Carlson, E. S.** (2012): Mixed convection in a lid-driven square cavity with an isothermally heated square blockage inside. *International Journal of Heat and Mass Transfer*, vol. 55, pp. 5244–5255.

**Kang, K. S.; Keyes, D. E.** (2008): Implicit symmetrized streamfunction formulations of magnetohydrodynamics. *International Journal for Numerical Methods in Fluids*, vol. 58, pp. 1201–1222.

**Kim, B. S.; Lee, D. S.; Ha, M. Y.; Yoon, H. S.** (2008): A numerical study of natural convection in a square enclosure with a circular cylinder at different vertical locations. *International Journal of Heat and Mass Transfer*, vol. 51, pp. 1888–1906.

**Le-Cao, K.; Mai-Duy, N.; Tran, C. D.; Tran-Cong, T.** (2011): Numerical study of stream-function formulation governing flows in multiply-connected domains by integrated RBFs and Cartesian grids. *Computers & Fluids*, vol. 44, pp. 32–42.

**Lima, J. A.; Rêgo, M. G. O.** (2013): On the integral transform solution of low-magnetic MHD flow and heat transfer in the entrance region of a channel. *International Journal of Non-Linear Mechanics*, vol. 50, pp. 25–39.

**Mejri, I.; Mahmoud, A.; Abbassi, M. A.; Omri, A.** (2014): MHD Natural Convection in a Nanofluid-filled Enclosure with Non-uniform Heating on Both Side Walls. *CMES - Computer Modeling in Engineering and Sciences*, vol. 10, pp. 83–114.

**Mramor, K.; Vertnik, R.; Sarler, B.** (2013): Simulation of Natural Convection Influenced By Magnetic Field with Explicit Local Radial Basis Function Collocation Method. *CMES - Computer Modeling in Engineering and Sciences*, vol. 92, pp. 327–352.

**Navarro, H. A.; Cabezas-Gómez, L.; Silva, R. C.; Montagnoli, A. N.** (2007): A generalized alternating-direction implicit scheme for incompressible magnetohydrodynamic viscous flows at low Reynolds number. *Applied Mathematics and Computation*, vol. 189, pp. 1601–1613.

**Oztop, H. F.; Zhao, Z.; Yu, B.** (2009): Fluid flow due to combined convection in lid-driven enclosure having a circular body. *International Journal of Heat and Fluid Flow*, vol. 30, pp. 886–901.

**Partridge, P. W.; Brebbia, C. A.; Wrobel, L. C.** (1992): *The dual reciprocity boundary element method*. Computational Mechanics Publications, Elsevier Science.

**Pekmen, B.; Tezer-Sezgin, M.** (2013): DRBEM Solution of Incompressible MHD Flow with Magnetic Potential. *CMES - Computer Modeling in Engineering and Sciences*, vol. 96, pp. 275–292.

**Rahman, M. M.; Alim, M. A.; Sarker, M. M. A.** (2010): Numerical study on the conjugate effect of joule heating and magneto-hydrodynamics mixed convection in an obstructed lid-driven square cavity. *International Communications in Heat and Mass Transfer*, vol. 37, pp. 524–534.

**Salah, N. B.; Soulimani, A.; Habashi, W. G.** (2001): A finite element method for magnetohydrodynamics. *Computer Methods in Applied Mechanics and Engineering*, vol. 190, pp. 5867–5892.

**Salah, N. B.; Soulimani, A.; Habashi, W. G.; Fortin, M.** (1999): A conservative stabilized finite element method for the magneto-hydrodynamics equations. *International Journal for Numerical Methods in Fluids*, vol. 29, pp. 535–554.

**Sentürk, K.; Tessarotto, M.; Aslan, N.** (2009): Numerical solutions of liquid metal flows by incompressible magneto-hydrodynamics with heat transfer. *International Journal for Numerical Methods in Fluids*, vol. 60, pp. 1200–1221.

**Sterl, A.** (1990): Numerical simulation of liquid-metal MHD flows in rectangular ducts. *Journal of Fluid Mechanics*, vol. 216, pp. 161–191.

